Structural investigation and Indium substitution in the thermoelectric $Mn_{2.7}Cr_{0.3}Si_4Al_{2-x}In_x$ series

Tristan Barbier[1], Emmanuel Combe[1], Ryoji Funahashi[1], Tomonori Takeuchi[1], Masataka Kubouchi[2], Yusuru Miyazaki[2], Emmanuel Guilmeau[3], Ryosuke O. Suzuki[4]

1- National Institute of Advanced Industrial Science and Technology (AIST), AIST Ikeda, Osaka 563-8577, Japan

2- Department of Applied Physics, School of Engeering, Tohoku University - 6-6-05, Aramaki Aza Aoba Aoba-ku, Sendai, Miyagi 980-8579, Japan

3- Laboratoire CRISMAT, UMR6508 CNRS ENSICAEN, 6bd Marechal Juin, 14050

4- Laboratory Eco-Processing, Division of Material Science, Graduate School of Engineering, Hokkaido University - N13W8, Kita-ku, Sapporo 060-8628, Japan

Corresponding author: funahashi-r@aist.go.jp

Keywords: Thermoelectric, Silicide compounds, Single crystals, X-Ray diffraction

Abstract:

Following the recent discovery of the promising $Mn_{2.7}Cr_{0.3}Si_4Al_2$ thermoelectric compound (applications such as automotive, industry, solar conversion…), a structural characterization through X-ray single crystal diffraction was performed. This layered material is composed of two distinct crystallographic sites where both (Mn, Cr) and (Al, Si) are randomly distributed. The crystallographic parameters deduced were then confirmed by powder X-ray diffraction through a temperature dependence of the phase stability, showing at the same time a chemical stability up to 873 K.

Taking into account the two distinct crystallographic sites highlighted, sample possessing two guest elements, one on each sites, were then synthesized in order to improve the thermoelectric properties. A solid solution has been found in the system $Mn_{2.7}Cr_{0.3}Si_4Al_{2-x}In_x$ with x varying from 0 to 0.2. Thus, double-substituted samples were studied through X-ray diffraction, electrical and thermal measurements. The present paper will describe and discuss the experimental results obtained.

Introduction:

Thermoelectric power generation provides a promising solution for close energy crisis and global climate change [1, 2]. Indeed, numerous sectors, such as automotive, industry, building, solar conversion and other, could take advantage of the thermoelectric materials capacity to directly convert the waste-heat into electrical energy. The overall performance of a thermoelectric material is determined by the dimensionless figure of merit $ZT = S^2.T/(\rho.\kappa_T)$, where S is Seebeck coefficient, T the absolute temperature, ρ the electrical resistivity and κ_T the total thermal conductivity [3]. Best performances, for low and medium temperature range (*i.e.* below 700 K), are currently obtained by the well-known Bi_2Te_3 compound with maximum ZT values around the unit (or higher) at 400 K, by $AgPb_mSbTe_{2+m}$ and Zn_4Sb_3 which exhibit ZT values higher than 1.70 and 1.35 at 700 K respectively [4]. However, the generally complex and costly synthesis procedures, together with the expensive, toxic and rare elements used, present serious impediments to large scale applications. Many efforts were therefore been made in order to find new environmentally-friendly, and efficient thermoelectric materials in the same temperature range. Based on this trend, silicon-based compounds appear as promising materials due to their both high abundance and non-toxicity. In 2013, Funahashi *et al.* [5] have highlighted the promising thermoelectric properties of $Mn_3Si_4Al_2$ through high Power Factor values ($PF = S^2/\rho$) and durable oxidation resistance (under air), in the middle temperature range (*i.e.* below 700 K). Indeed, efficient thermoelectric materials should not be described only by high ZT values, ageing materials evaluation must be also considered (*i.e.* time dependence of the chemical stability), especially for usual applications where environmentally conditions such as

humidity, temperature or atmospheric pollution, can strongly affect the efficiency of the thermoelectric materials. Following these results, thermoelectric properties improvement has been studied via some substitutions on the manganese site. Best performances were obtained with a chromium substitution ($Mn_{2.7}Cr_{0.3}Si_4Al_2$) leading to a *ZT* value of 0.30 at 573 K [6].

As mentioned above, $Mn_{2.7}Cr_{0.3}Si_4Al_2$ appears like a promising candidate for thermoelectric generator applications [6]. However, its thermal conductivity, from 4 to 7 $W.m^{-1}.K^{-1}$ at room temperature and 700 K respectively, might be reduced in order to improve the thermoelectric properties. For that purpose, thermal conductivity mechanisms must be fully understood. Thus, a structural investigation of $Mn_{2.7}Cr_{0.3}Si_4Al_2$ using single crystal and powder X-ray diffraction will be described in the present paper. The temperature dependence of the phase stability will be also discussed in order to confirm the temperature range where this material could be used. Finally, a new way for decreasing the thermal conductivity, using simultaneously two guest elements will be presented and discussed.

Experimental:

Synthesis

$Mn_{2.7}Cr_{0.3}Si_4Al_{2-x}In_x$ with x varying from 0 to 1 was prepared using the following chips precursors (Alpha Aesar): Mn (99.9 %), Cr (99.9 %), Si (99.999 %), In (99.9 %) and $Al_{76}Si_{24}$ alloy. Aluminium-silicon alloy was used in order to obtain a more accurate composition of the final ingots. Indeed, the melting-point difference between the main

precursors, especially aluminium, leads to imprecise nominal compositions. Following twenty minutes of vacuum process, ingots were obtained using arc melting process. After removing, by polishing, of the oxidized surfaces of the resulting ingots, pulverulent powders were obtained by mechanical crushing. The resulting powders, sieved down to 200 μm, were then shaped and densified in one time, using Spark Plasma Sintering (*SPS*), at 1023 K for 30 min (heating and cooling rate of 100 K/min) under a pressure of 50 MPa using graphite dies of 15 mm diameter. The final thickness of the pellets was around 5 mm with a density in excess of 95 % of the crystallographic value.

Characterizations techniques:

Single-crystal X-ray diffraction was performed using $Mn_{2.7}Cr_{0.3}Si_4Al_2$ crystals, pick up from the powder. Typical size of the crystal was 0.9 x 0.9 x 0.8 mm^3. Diffraction data were then collected on a single crystal X-ray diffractometer, Bruker Quest using Mo K_α radiation (λ_1 = 0. 71073 Å, λ_2 = 0. 70930 Å), equipped with the PHOTON 100 CMOS detector. The unit cell parameters were refined during the integration with the ShelXS-97 program [7]. Face indexed analytical absorption correction was applied to the collected diffraction intensity data. The crystal structure refinement was performed using JANA2006 [8] and the crystal structure was drawn using Diamond 3.2.

High Resolution X-Ray powder Diffraction (*HRXRD*) data of $Mn_{2.7}Cr_{0.3}Si_4Al_2$ against temperature, from room temperature up to 873 K were collected using a D8 Advance Vario 1 Bruker two-circle diffractometer ($\theta - 2\theta$ Bragg-Brentano mode) using Cu K_α radiation (λ = 1.540598 Å) with a Ge (111) monochromator (Johansson type) and a Lynx Eye detector.

High-temperature experiments were carried out with an Anton Paar furnace HTK1200N; the temperature was regulated within ± 3 K. Data were collected over the angular range $8 \leq 2\theta/° \leq 100$ counting for 0.8 s at each angular increment of 0.0105° (2 h/scan). Isothermal XRD patterns were recorded every 50 K from 373 to 873 K (heating rate of 30 K/min). A diffraction pattern of a standard powder LaB_6 was also recorded in order to determine the instrumental broadening of diffraction peaks. The angular dependence of the Full Width at Half Maximum (*FWHM*) of the diffraction peaks obtained from LaB_6 was determined using both the Caglioti *et al.* function ($FWHM(\theta) = (U \tan^2\theta + V \tan\theta + W)^{1/2}$, where U, V and W are to be refined [9]) for the Gaussian component and the parameters *X* and *Y* for the Lorentzian contribution. The resulting Lorentzian and Gaussian contributions to the *FWHM* of the diffraction peaks were used as instrumental parameters for the Rietveld refinements.

The polycrystalline phases of $Mn_{2.7}Cr_{0.3}Si_4Al_{2-x}In_x$ ($0 < x < 1$) were identified at room temperature by powder X-Ray Diffraction (*XRD*) using refined structural parameters of the single-crystal sample. Data were collected using a RINT2000-TTR two-circle diffractometer (θ–2θ Bragg-Brentano mode) using Cu K_α radiation ($\lambda = 1.540598$ Å). Data were then collected over the angular range $8 \leq 2\theta/° \leq 100$ with a step size of 0.010°, and a step time of 2s.

The full-profile-fitting refinements of both *HRXRD* against temperature and $Mn_{2.7}Cr_{0.3}Si_4Al_{2-x}In_x$ series at room temperature were performed using the Rietveld method from the *FullProf* and *WinPlotr* software packages [10, 11]. The shape of the diffraction peaks was modeled using a Thompson-Cox-Hastings pseudo-Voigt profile function [12]. Zero-point shift and asymmetry parameters were systematically refined, and the

background contribution was estimated manually. Lattice parameters, fractional atomic coordinates and isotropic displacement parameters (*i.e.* Debye-Waller factors: B_{iso}), were finally refined. It can be also mentioned that the site occupancies were fixed for all atoms.

Temperature dependence of resistivity and Seebeck coefficient were measured from two polycrystalline rectangular bars (3.5 x 3.5 x 10 mm^3), beforehand polished with sandpaper in order to avoid any pollution. The Seebeck coefficient (S) values were calculated from a plot of thermoelectric voltage against the temperature differential as measured from 373 up to 900 K in air using an instrument designed by our laboratory. Two Pt - Pt/Rh (R-type) thermocouples, used also for voltage terminals, were adhered to both ends of the samples using silver paste. Measured thermovoltage was plotted against the temperature difference and the slope corresponds to the apparatus Seebeck coefficient.

Electrical resistivity (ρ) was measured using the standard DC four probes method in air from room temperature up to 900 K. Silver paste was used for the connections between the samples and both the current and voltage lead wires.

The heat capacity and thermal diffusivity were analyzed over the same temperature range using a laser Flash device. The thermal conductivity (κ_{total}) was determined using the product of the measured density, the thermal diffusivity, and the theoretical heat capacity, using Dulong-Petit approximation. The lattice thermal conductivity was determined from the Wiedemann-Franz law by subtracting the electronic contribution to the thermal conductivity from the total thermal conductivity ($\kappa_{lattice} = \kappa_{total} - \kappa_{elec}$).

Hall effect experiments were carried out at room temperature in order to determine the carrier concentration. The specimens were prepared by polishing the sintered samples and cutting them into plate-like squares with the dimensions of 3 x 3 mm^2 and 0.3 mm in thickness. Conductive epoxy contacts were deposited on the four corners of the square sample. By applying a longitudinal electric field (current flow I = 5 mA) between two opposite corners and a perpendicular magnetic field (from 7 T to -7 T), Hall resistance (R_H) and voltage (V_H) or transverse voltage were measured between the two other corners. The carrier concentration *n* was then calculated from the fit of the V_H(B) curve according to the following equation:

$$V_H = \mathrm{I}\left(\alpha B^2 + \frac{IB}{nqt} + c\right) \quad (1)$$

Where *q* is the negative charge of the electron and *t* the thicknesses of the square samples. The constant term c and the quadratic term originate from the small misalignment of the voltage contacts.

Results and discussion:

$Mn_{2.7}Cr_{0.3}Si_4Al_2$

In order to investigate the detailed crystal structure of $Mn_{2.7}Cr_{0.3}Si_4Al_2$, single-crystal X-ray measurements were performed from single crystal, which was pick up, from powder of the densified pellets. Details of the data collection and structure refinements of $Mn_{2.7}Cr_{0.3}Si_4Al_2$ phase are gathered in **Table I.** $Mn_{2.7}Cr_{0.3}Si_4Al_2$ phase crystallizes in the hexagonal $CrSi_2$-type (C40) structure (space group $P6_222$ n° 180). The Rietveld modelling leads to cell parameters and atom coordinates which were gathered in the **table I**. It can be pointed out

that the unit cell parameters deduced in this study (***a*** = 4.469(1) Å and ***c*** = 6.425(1) Å) are in well agreement with those previously published (***a*** = 4.447(1) Å; ***c*** = 6.433(1) Å) [6]. The refinement highlights two distinct atomic positions, one for Mn and as expected Cr; another atomic position was determined for both silicon and alumina. The single crystal X-ray diffraction measurement did not allowed to determine any periodicity of Al and Si, we consequently assumed a random distribution of these atoms on the same crystallographic site. $Mn_{2.7}Cr_{0.3}Si_4Al_2$ can therefore be described as a structure containing three hexagonal layers, which are rotated against each other around the screw axis by 60°. Each layer consists of repeating atom rows with (Mn, Cr) – (Al, Si) – (Al, Si) – sequence (see Figure 1, right).

In order to confirm the crystallographic parameters of $Mn_{2.7}Cr_{0.3}Si_4Al_2$ deduced by single crystal X-ray refinement, powder X-ray diffraction analysis was performed at room temperature (**Figure 1).** A schematic representation of $Mn_{2.7}Cr_{0.3}Si_4Al_2$ unit-cell is depicted in Figure 1 as well (right part)**.** Pattern displayed in **Figure 1** shows single phase and well crystallize compound, through a well-agreement between the calculated Bragg positions with those of the experimental peaks, as it can be observed through the (blue) bottom line which show the difference between the experimental and the calculated data. The perfect fit between the experimental data and the calculated ones confirms the deduced crystallographic parameters. According to the atomic coordinates deduced by single crystal X-ray diffraction and those given in the literature for $CrSi_2$, we have chosen the following coordinates for all powder refinements: Mn, Cr: (1/2, 0, 0) – Al, Si: (1/6, 1/3, 0) (**Table II**).

The temperature dependence of the $Mn_{2.7}Cr_{0.3}Si_4Al_2$ phase stability was also studied through powder XRD analyses in the temperature range of RT to 873 K (**Figure 2**). All patterns displayed in **Figure 2** show single phase samples. No additional peaks or intensities modifications can be observed from room temperature up to 873 K; showing a good phase stability up to 873 K. The Rietveld modelisation of all these patterns, using the aforementioned crystallographic parameters, have led to deduce the unit cell parameters ***a*** and ***c***. The temperature dependence of the unit cell parameters is displayed in **Figure 3**. It can be observed a logical increase of both ***a*** and ***c*** cell parameters from 4.471(1) Å at room temperature to 4.515(1) Å at 873 K and from 6.438(1) Å to 6.491(1) Å for the **a** and **c** cell parameters respectively. These increases can safely be attributed to the increase of the thermal motion of all atoms. These results also confirm the great stability of $Mn_{2.7}Cr_{0.3}Si_4Al_2$ up to 873 K.

$Mn_{2.7}Cr_{0.3}Si_4Al_{2-x}In_x$ series

Highlighting the two distinct atomic coordinates, a new approach for optimizing the thermoelectric properties of $Mn_{2.7}Cr_{0.3}Si_4Al_2$ could be considered. Indeed, a double substitution, one on each crystallographic site, should induce an optimization of the charge carrier concentration while the thermal conductivity can be reduced, at the same time, through a decrease of the lattice component due to the crystallographic disorder induced by the guest atoms. For that purpose, $Mn_{2.7}Cr_{0.3}Si_4Al_{2-x}In_x$ samples, with x = 0, 0.05, 0.10, 0.15, 0.20, 0.40, 0.60, 0.80 and 1.00 were synthesized, densified and studied. The XRD patterns recorded at room temperature from powders of the obtained SPS pellets for all ***x***

values are displayed in **Figure 4**. These patterns show that, for all x values in the range $0 \leq x \leq 0.20$, a phase derived from $Mn_{2.7}Cr_{0.3}Si_4Al_2$ is mainly obtained (**Figure 4 left**). However, it can be observed at $2\theta = 41.8°$ and 49° peak-shoulders; the intensity of these latter peaks increase with the indium content. As these extra-peaks are only observed on two peaks, any Al or In-rich phases may not be considered; they have therefore been assumed to correspond to an impurity. However the low intensities of the peak-shoulders did not allow determining nature or composition. All XRD patterns were well described by the hexagonal space group $P6_222$ (n° 180) of the $Mn_3Si_4Al_2$ host structure [6]. For an indium content higher than 0.20 some secondary phases, pointed out by # and * in the **Figure 4 right**, respectively In and $MnSi_{\sim 1.75}$, can be observed. A solubility limit of indium ≤ 0.20 was found in the present double substitution case. The decrease of the Al content may lead to the $Mn_{2.7}Cr_{0.3}Si_4Al_{2-x}In_x$ phase decomposition; indeed, the peak intensities of both secondary phases increase with the increase of the indium content, while the intensities of $Mn_{2.7}Cr_{0.3}Si_4Al_{2-x}In_x$ peaks decrease relatively. However $Mn_{2.7}Cr_{0.3}Si_4Al_{2-x}In_x$ phase is still present for $x = 1$. Due to both, small amount of indium and the random distribution of Mn, Cr and Al, Si and In, occupancies of all atoms were fixed during the refinements. Substitution results in a systematic expansion of the unit-cell axis and of the unit-cell volume (**Figure 5**). The ***a*** and ***c*** parameters increase from 4.471(1) and 6.440(1) Å for $\boldsymbol{x} = 0.05$ to 4.480(1) and 6.462(1) Å for $\boldsymbol{x} = 1.0$. It seems that even if the phase decomposition occurs, some indium atoms are still substituted instead of Al. The linear increase of both unit cell parameters (***a*** and ***c***) follow the Vegard's law and considering the

metallic radii of these two elements (r_{Al} = 143 pm, r_{In} = 167 pm), we can concluded that indium is correctly substituted instead of Al [13].

Thermoelectric properties

The relative density values, gathered in the **Table III**, highlight a slight increase of those values with the indium content. Indeed, values increase from 96.7 % to 98 % for x = 0.05 and 0.20 respectively. As the sintering process was similar for all samples, it would seem that indium facilitates the grain arrangement thus improving the density. The temperature dependences of the electrical resistivity, the Seebeck coefficient and total thermal conductivity in the $Mn_{2.7}Cr_{0.3}Si_4Al_{2-x}In_x$ series with $0 \leq \boldsymbol{x} \leq 1$, are display in **Figure 6.** Resistivity, Seebeck coefficient and total thermal conductivity curves, collected from room temperature up to 900 K, clearly demonstrate two behaviors, for single phase and multiphase samples respectively. An indium content, higher than the solubility limit (x > 0.2), seems to induce a decomposition of $Mn_{2.7}Cr_{0.3}Si_4Al_{2-x}In_x$ into $MnSi_{\sim 1.75}$ and In. As the secondary phase $MnSi_{\sim 1.75}$ exhibits a *p*-type response, the thermoelectric properties of $Mn_{2.7}Cr_{0.3}Si_4Al_{2-x}In_x$ (x > 0.2) are clearly affected, especially the Seebeck coefficient.

All curves, in the series $Mn_{2.7}Cr_{0.3}Si_4Al_{2-x}In_x$ ($0 \leq x \leq 0.2$), reach a maximum as shown in **Figure 6**. These bell-shape curves describe an evolution from a metal-like behavior to an insulator one at higher temperature; these changes can be explained by an intrinsic transition [6].

It can be observed on the resistivity curves (**Figure 6a)**, a clear tendency towards more insulating behavior for the multiphase samples. For instance, at 750 K, the resistivity of the

multiphase samples reach values between 2.26 and 2.80 mOhm.cm, while the single phase samples exhibit values between 1.2 and 1.4 mOhm.cm at the same temperature. These two behaviors may be explained by the $MnSi_{\sim 1.75}$ secondary phases content increase, which possess a resistivity close to 5 mOhm.cm at 700 K [14]. A slight increase of the resistivity is observed for the single phase samples, from 1.00 mOhm.cm to 1.35 mOhm.cm for x = 0 and 0.20 samples respectively. Hall effects measurements were performed to determine the electron concentration, for single phase samples, at 300 K (gathered in **Table III**). In agreement with the existence of the solid solution, the carrier concentration decrease linearly (from 5.10×10^{21} to 2.70×10^{21} cm^{-3} for an indium content of 0.05 and 0.20 respectively) with the indium content increase, explaining the slight increase of the resistivity.

Figure 6b shows temperature dependence of the Seebeck coefficient. The absolute value of the Seebeck coefficient decreases from 73 to 41 $\mu V.K^{-1}$ for x = 0 to 0.20 samples respectively (at 623 K), since carrier concentration *n* decreases. Even if the Seebeck coefficient is less affected by the density, the decrease of the charge carrier concentration could not explained the decrease of the Seebeck coefficient values. Different hypotheses could be assumed in order to explain the observed behavior; however the most suitable concerned the peak-shoulders observed (see structural part). Indeed, the assumed impurity may distort the measured values, especially if this secondary phase exhibits a *p*-type response. For instance, the *p*-type $MnSi_{\sim 1.75}$ compound exhibits Seebeck value around +180 $\mu V.K^{-1}$ at 623 K [15]. The strong influence of the *p*-type $MnSi_{\sim 1.75}$ can be observed for the

substituted compounds with x > 0.4, where the Seebeck coefficient turns to the positive values at high temperature.

The temperature dependence of the total thermal conductivity for $Mn_{2.7}Cr_{0.3}Si_4Al_{2-x}In_x$ was depicted in **Figure 6c.** The thermal conductivity curves also show two behaviors. An increase of the thermal conductivity with the indium content can be observed for the single phase samples (from 5.33 to 6.55 $W.m^{-1}.K^{-1}$ for $\boldsymbol{x}$ = 0.05 and 0.20 respectively, at 623 K) while a decrease can be observed for the multiphase samples (from 5.33 to 3.50 $W.m^{-1}K^{-1}$ at 623 K). As well as resistivity and Seebeck coefficient curves, these two behaviors can be attributed to $MnSi_{\sim 1.75}$ secondary phases which exhibits a thermal conductivity value around 2.2 $W.m^{-1}.K^{-1}$ at 623 K [15]. An increase of the secondary phase content therefore explained the drastic decrease of the total thermal conductivity observed for the multiphase samples.

In the case of the single phase samples, as aforementioned, the density difference between these samples can explain the thermal conductivity. As the total thermal conductivity of these compounds is mainly governed by the lattice component, the increase of this latter, due to the increase of the mobility (gathered in the **Table III**) can explained the behavior of the total thermal conductivity. Nevertheless, the electronic contribution gathered in **Table III,** slightly decreases with the indium content increase, due to the decrease of the charge carrier concentration, but do not modify strongly the total response.

Compared to the $Mn_{2.7}Cr_{0.3}Si_4Al_2$ compounds, the indium substitution leads to increase the resistivity and in the same way, leads to decrease the electronic part of the thermal conductivity. However, the drastic decrease of the absolute Seebeck coefficient, together

with an increase of the lattice part of the thermal conductivity induce a degradation of both power factor and figure of merit ZT (Figure 7).

Conclusion:

Structural characterization of the promising $Mn_{2.7}Cr_{0.3}Si_4Al_2$ thermoelectric compound was studied in the present paper through single crystal and X-ray diffraction. The crystallographic structure of this compound can be described as a structure containing three hexagonal layers, which are rotated against each other around a screw axis by 60°; where each layers consist of repeating atom rows with Mn, Cr - Al, Si - Al, Si - sequence, with a random distribution of Mn, Cr and Al, Si on the two distinct crystallographic sites.

Temperature dependence of the phase stability through powder X-ray diffraction, led, on one hand, to confirm the crystallographic parameters deduced by single crystal X-ray diffraction and, on another hand, to highlight phase stability up to 873 K.

After showing the two distinct crystallographic sites of $(Mn, Cr)_3(Si, Al)_6$, samples containing two guest elements where synthesized, Cr on the Mn site and In on the Al, Si site. A solubility limit of $x \leq 0.2$ was highlighted; however, a drastic decrease of the absolute Seebeck coefficient values avoids an optimization of the thermoelectric properties.

Nevertheless, the solid solution highlighted in the present paper, may lead to a new way for decreasing the total thermal conductivity and therefore improving the thermoelectric properties.

Table I: Crystal Data and Data Collection Parameters for $Mn_{2.7}Cr_{0.3}Si_4Al_2$

Crystal data		***Data collection***	
Chemical formula	$Mn_{2.6(4)}Cr_{0.3(1)}Si_{4.0(1)}Al_{1.9(8)}$	Diffractometer	Bruker Quest
Formula weight ($g.mol^{-1}$)	330.24	Radiation type	Mo Kα
Temperature (K)	293	θ range for data collection (°)	5.26 - 42.02
Crystal size (mm^3)	0.9 x 0.9 x 0.8	Absorption coefficient (mm^{-1})	9.597
Crystal color	Black	Index ranges	$-8 \leq h \leq 8$
			$-8 \leq k \leq 8$
			$-12 \leq l \leq 12$
Crystal system, space group	Hexagonal, $P6_222$	Reflections collected / unique	2191 / 1252
Z	18		
Unit-cell	a = b = 4.469(1) Å	Data/restrains/parameters	1252 / 8 / 267
	c = 6.425(1) Å	Goodness-of-fit obs / all	1.00 / 0.98
	α = β = 90.0 °	Final R indices, R_1 / wR_2	0.0197 / 0.0350
	γ = 120.0 °	R indices (all data), R_1 / wR_2	0.0401 / 0.0399
Volume ($Å^3$)	157.20		

Atomic coordinates			
Mn, Cr (x, 0, 0)	0.5		
Al, Si (x, 2x, 0)	0.1647, 0.3294		

Table II: Crystallographic parameters of $Mn_{2.7}Cr_{0.3}Si_4Al_2$ deduced from powder X-ray Rietveld refinement at room temperature.

$Mn_{2.7}Cr_{0.3}Si_4Al_2$	$P6_222$				
	a = 4.471(1) Å, c = 6.438(1) Å χ^2 = 2.243 ; R_{Bragg} = 7.06 ; R_F = 7.62				
	x	y	z	Biso (Å^2)	Occupancy
Mn	½	0.0	0.0	0.749(1)	0.90
Cr	½	0.0	0.0	0.749(1)	0.10
Si	1/6	1/3	0.0	0.225(1)	0.66
Al	1/6	1/3	0.0	0.225(1)	0.33

Table III: c cell parameter, carrier concentration (n) and mobility (μ) at 300 K, electrical resistivity (ρ), Seebeck coefficient (S), thermal conductivity (κ_{total}), its lattice ($\kappa_{lattice}$) components at 623 K in $Mn_{2.7}Cr_{0.3}Si_4Al_{2-x}In_x$ single phase compounds ($x < 0.4$).

x	**a unit-cell parameter (Å)**	**c unit-cell parameter (Å)**	**Relative density (%)**	**ρ (mOhm.cm)**	**S (μV/K)**	**κ_{total} (W/mK)**	**$\kappa_{lattice}$ (W/mK)**	**μ ($cm^2.V^{-1}.s^{-1}$)**	**n (x 10^{21} cm^{-3})**
0.05	4.4711	6.4407(1)	96.7	1.25	-56	5.33	4.12	0.98	5.10
0.10	4.4721	6.4404(1)	97.1	1.23	-62	5.39	4.15	1.18	4.30
0.15	4.4735	6.4446(1)	97.3	1.33	-48	6.14	4.99	1.26	3.70
0.20	4.4725	6.4434(1)	98.0	1.35	-41	6.55	5.43	1.71	2.70

Captions:

Figure 1: (left side) Powder X-ray diffraction pattern of $Mn_{2.7}Cr_{0.3}Si_4Al_2$ measured at room temperature; observed (red solid line) and calculated (black circles) data. The difference profile is shown at the bottom (blue solid lines). (right side) schematic representations of the $Mn_{2.7}Cr_{0.3}Si_4Al_2$ unit-cell.

Figure 2: Powder X-ray diffraction patterns of $Mn_{2.7}Cr_{0.3}Si_4Al_2$ in the temperature range $RT \leq T/K \leq 873$.

Figure 3: Temperature dependence of **a** and **c** unit cell parameters of $Mn_{2.7}Cr_{0.3}Si_4Al_2$.

Figure 4: Experimental and calculated powder X-ray diffraction data of $Mn_{2.7}Cr_{0.3}Si_4Al_{2-x}In_x$ with x varying from 0.05 to 0.20 (left side) and from 0.40 to 1.00 (right side). The # and * pointed out the secondary phases of In and $MnSi_{\sim 1.75}$ respectively.

Figure 5: Variation of a and c unit cell parameters versus x in the $Mn_{2.7}Cr_{0.3}Si_4Al_{2-x}In_x$ series

Figure 6: Temperature dependence of the a) electrical resistivity, b) Seebeck coefficient and c) thermal conductivity of the $Mn_{2.7}Cr_{0.3}Si_4Al_{2-x}In_x$ series.

Figure 7: Temperature dependence of the power factor and figure of merit ZT, in the $Mn_{2.7}Cr_{0.3}Si_4Al_{2-x}In_x$ series.

References:

[1] G. A. Slack, in CRC, "*Handbook of thermoelectric"*, edited by D.M. Rowe (CRC, Boca Raton) (1995) 407

[2] G. J. Snyder, E. S. Toberer, Nature Mater., 7 (2008) 105 – 114

[3] G. S. Nolas, J. Sharp, H. J. Goldsmid, Springer, New York (2001)

[4] T. M. Tritt and M. A. Subramanian, MRS Bulletin, 31 (2006)

[5] R. Funahashi, Y. Matsumura, T. Takeuchi, H. Tanaka, W. Norimatsu, E. Combe, R. O. Suzuki, C. Wan, Y. Wang, M. Kusunoki, K. Koumoto, Mater. Res. Soc. Symp. Proc. 1490 (2013)

[6] R. Funahashi, Y. Matsumura, H. Tanaka, T. Takeuchi, W. Norimatsu, E. Combe, R. O. Suzuki, Y. Wang, C. Wan, S. Katsuyama, M. Kusunoki, K. Koumoto, J. Appl. Physics, 112 (2012) 073713

[7] G. M. Sheldrick, Acta Cryst. A64 (2008) 112-122

[8] V. Petricek, M. Dusek, L. Palatinus, Z. Kristallogr., 229 (2014) 5, p 345-352

[9] G. Caglioti, A. Paoletti and F.P. Ricci, Nuclear Instrument, 3 (1958) 223-228

[10] J. Rodriguez-Carvajal, *Physica B*, **192** (1993), pp 55-59

[11] T. Roisnel, J. Rodriguez-Carvajal, Mater. Sci. Forum, 378-381 (2001), pp 118-123

[12] P. Thompson, D.E. Cox and J.B. Hastings, J. Appl. Cryst., 20 (1987), pp 79-83

[13] http://www.webelements.com/periodicity/metallic_radius/

[14] Y. Kikuchi, Y. Miyasaki, Y. Saito, K. Hayashi, K. Yubuta, T. Kajitani, Jap. J. Appl. Phys., 51 (2012) 085801

[15] Z. Zamanipour, X. Shi, M. Mozafari, J. S. Krasinski, L. Tayebi, D. Vashaee, Ceramics International 39 (2013) 2353-2358

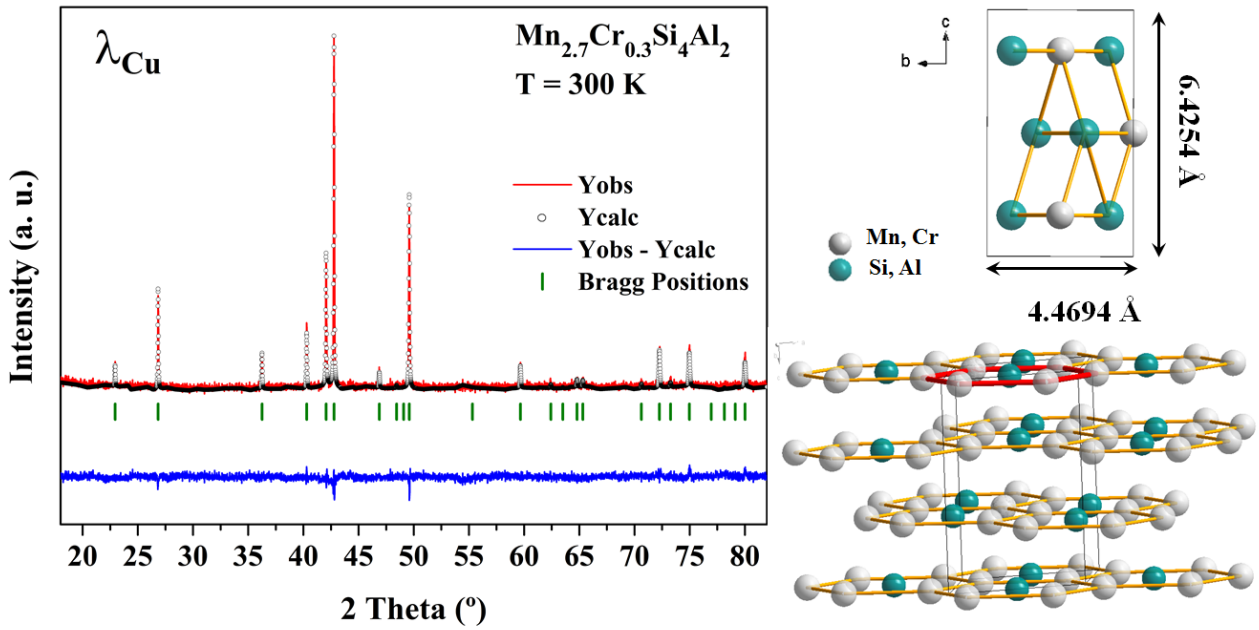
λCu
Mn2.7Cr0.3Si4Al2
T = 300 K
Yobs
Ycalc
Yobs - Ycalc
Bragg Positions
Intensity (a. u.)
2 Theta (°)
20 25 30 35 40 45 50 55 60 65 70 75 80
c
b
6.4254 Å
Mn, Cr
Si, Al
4.4694 Å

Figure 1:

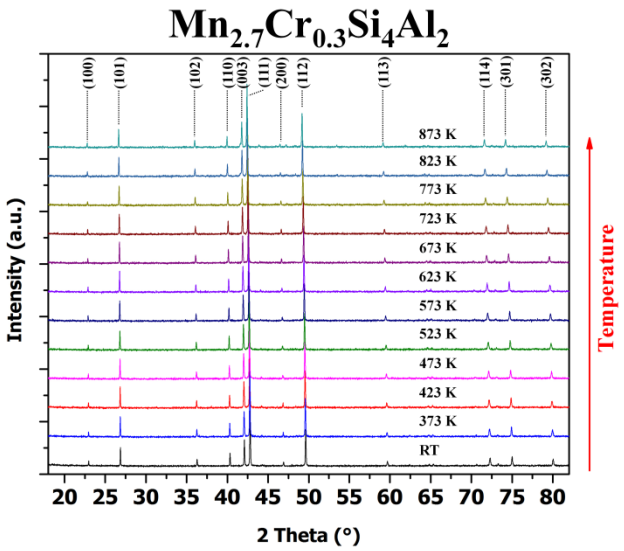
Mn2.7Cr0.3Si4Al2
(100)
(101)
(102)
(110)
(003)
(111)
(200)
(112)
(113)
(114)
(301)
(302)
873 K
823 K
773 K
723 K
673 K
623 K
573 K
523 K
473 K
423 K
373 K
RT
Intensity (a.u.)
2 Theta (°)
20 25 30 35 40 45 50 55 60 65 70 75 80
Temperature

Figure 2:

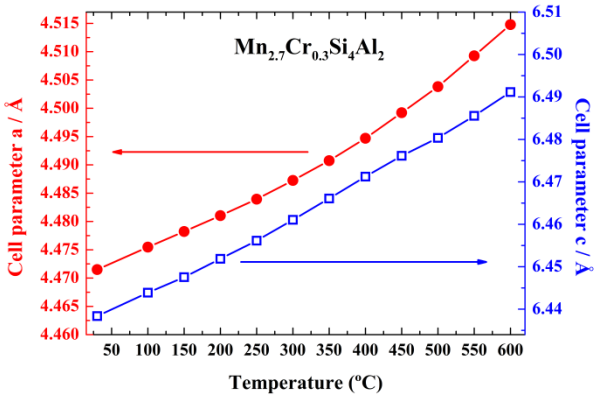
Mn2.7Cr0.3Si4Al2
Cell parameter a / Å
Cell parameter c / Å
Temperature (°C)
4.515
4.510
4.505
4.500
4.495
4.490
4.485
4.480
4.475
4.470
4.465
4.460
6.51
6.50
6.49
6.48
6.47
6.46
6.45
6.44
50 100 150 200 250 300 350 400 450 500 550 600

1

2 Figure 3:

3

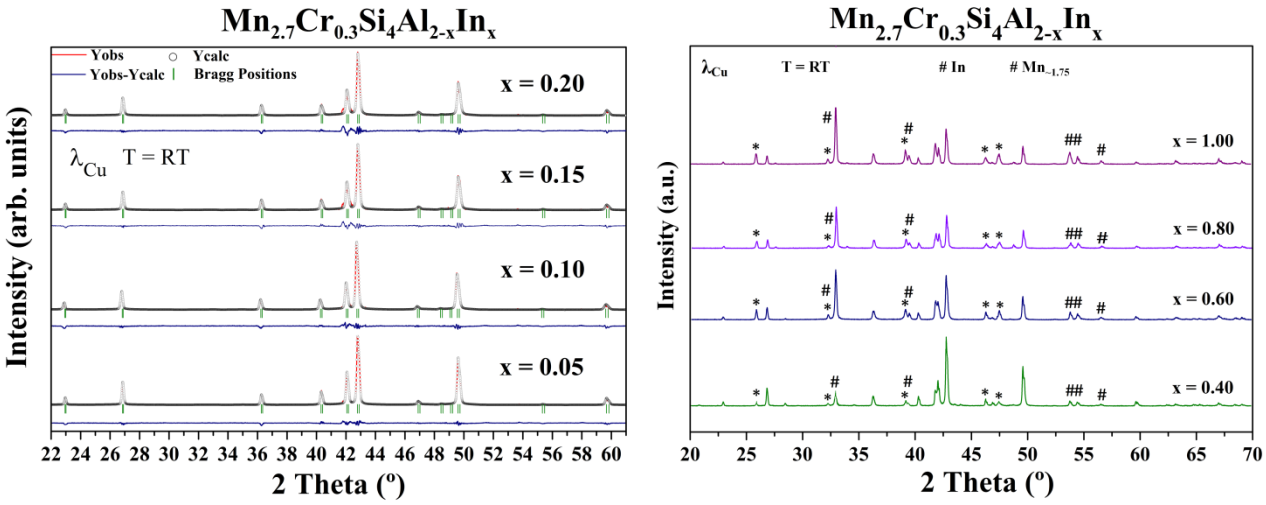
Mn2.7Cr0.3Si4Al2-xInx
Yobs
Ycalc
Yobs-Ycalc
Bragg Positions
λCu T = RT
x = 0.20
x = 0.15
x = 0.10
x = 0.05
Intensity (arb. units)
2 Theta (°)
Mn2.7Cr0.3Si4Al2-xInx
λCu T = RT
# In
# Mn~1.75
x = 1.00
x = 0.80
x = 0.60
x = 0.40
Intensity (a.u.)
2 Theta (°)

Figure 4:

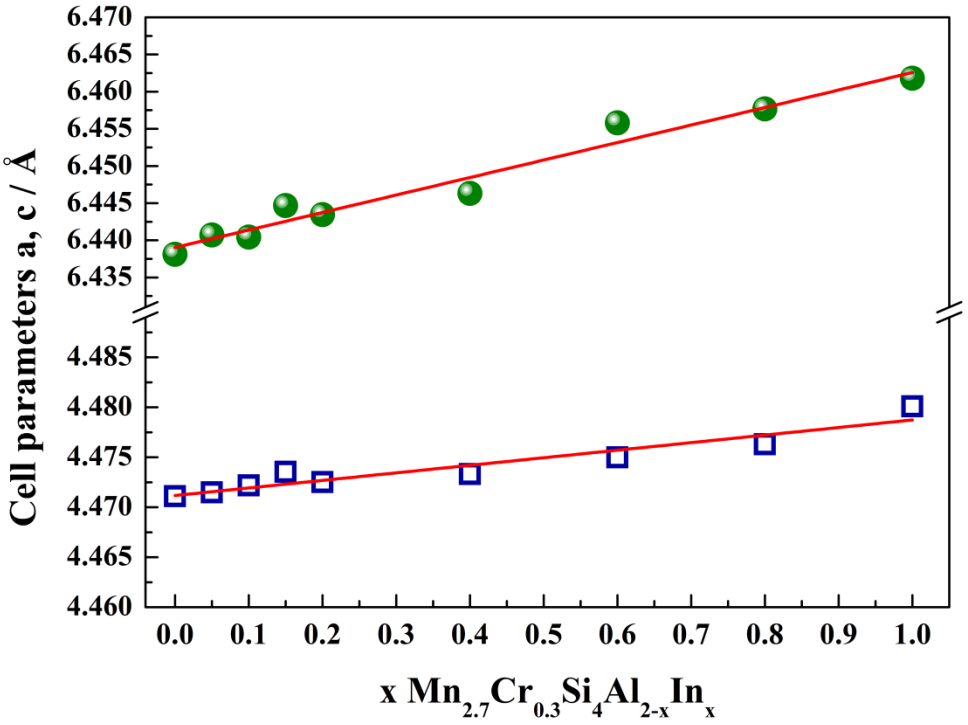
Cell parameters a, c / Å
6.470
6.465
6.460
6.455
6.450
6.445
6.440
6.435
4.485
4.480
4.475
4.470
4.465
4.460
0.0
0.1
0.2
0.3
0.4
0.5
0.6
0.7
0.8
0.9
1.0
x Mn2.7Cr0.3Si4Al2-xInx

Figure 5:

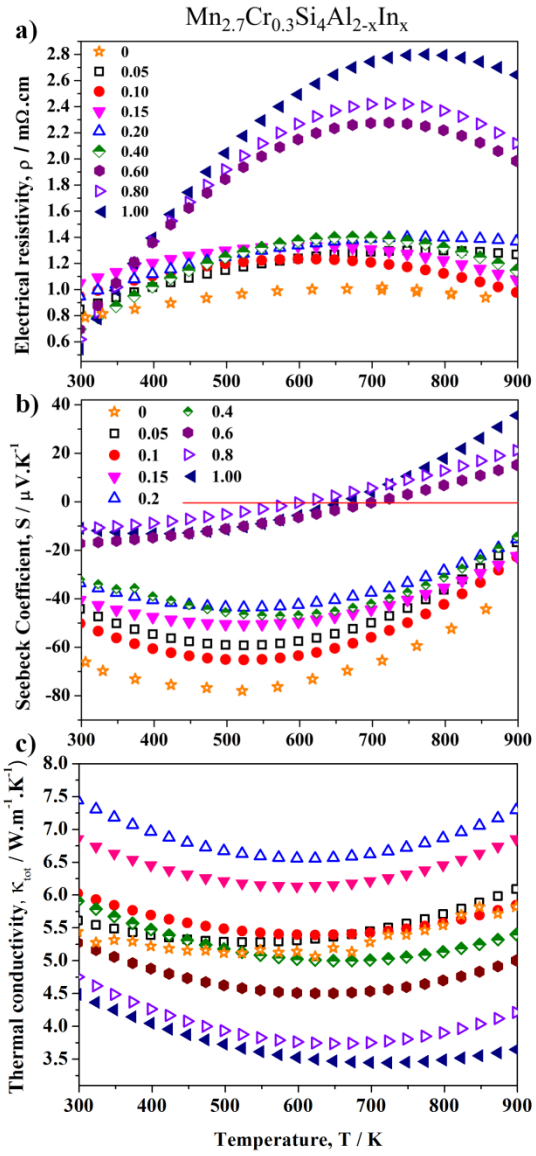
Mn2.7Cr0.3Si4Al2-xInx
a)
Electrical resistivity, ρ / mΩ.cm
0
0.05
0.10
0.15
0.20
0.40
0.60
0.80
1.00
b)
Seebeck Coefficient, S / μV.K-1
0
0.05
0.1
0.15
0.2
0.4
0.6
0.8
1.00
c)
Thermal conductivity, κtot / W.m-1.K-1
Temperature, T / K

Figure 6:

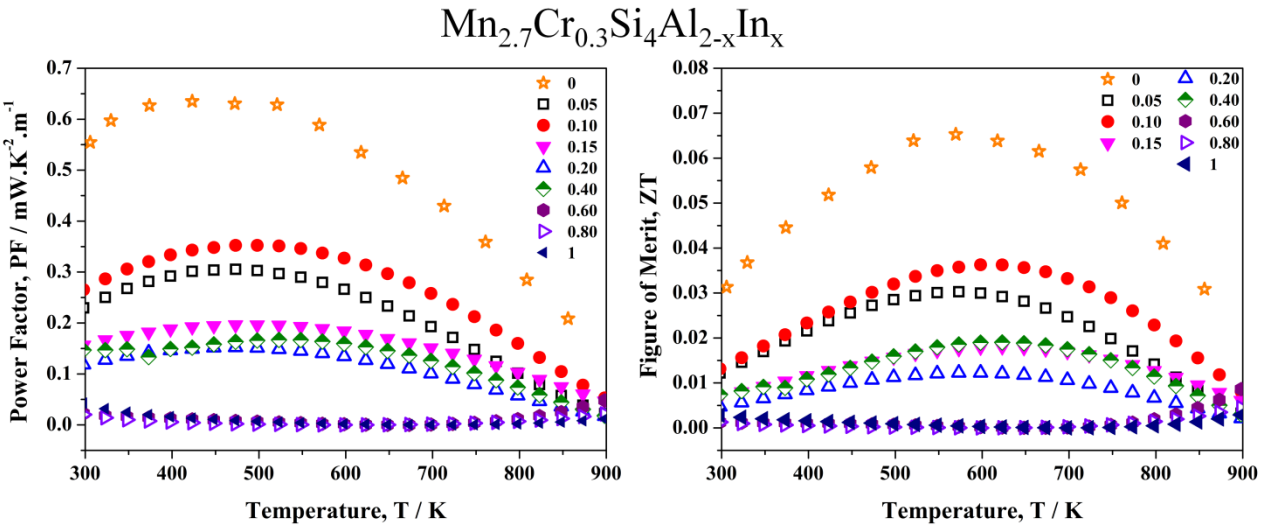
Mn2.7Cr0.3Si4Al2-xInx
Power Factor, PF / mW.K-2.m-1
Temperature, T / K
Figure of Merit, ZT
Temperature, T / K
0
0.05
0.10
0.15
0.20
0.40
0.60
0.80
1

Figure 7: